BNL-77935-2007-JA

MICROPHYSICAL PROPERTIES OF STRATUS/STRATOCUMULUS CLOUDS DURING THE 2005 MARINE STRATUS/STRATOCUMULUS EXPERIMENT (MASE)

P. H. Daum, Y. Liu, R. L. McGraw, Y.-N. Lee, J. Wang, G. Senum, and M. Miller,
Atmospheric Sciences Division, Brookhaven National Laboratory, Upton, NY

and

J. G. Hudson
Desert Research Institute, Reno, NV

April 2007

Submitted to
J. Geophys. Res.

Environmental Sciences Department/Atmospheric Sciences Division

Brookhaven National Laboratory
P.O. Box 5000
Upton, NY 11973-5000
www.bnl.gov

ABSTRACT

Properties of marine stratus/stratocumulus clouds were measured over the Eastern Pacific Ocean during the month of July 2005 using the Department of Energy G-1 aircraft. Flights were conducted over a coastal site located at Pt Reyes National Seashore just north of San Francisco, and extended west over the Pacific Ocean to as far as 200 km offshore, and as far south as Monterey Bay. Clouds sampled during these flights extended from near the ocean surface to altitudes between 300 and 450 m, (msl). In all cases cloud top was associated with a strong temperature inversion. Liquid water content (LWC) increased nearly linearly with altitude from cloud-base to cloud-top, but on six of the seven cloud flights, the liquid water path was sub-adiabatic. Layer-averaged cloud droplet number concentrations (CDNC) ranged between 90 cm^{-3} and 350 cm^{-3} and were clearly an increasing function of pre-cloud accumulation-mode aerosol number concentrations. The fraction (F_a) of particles with $d > 0.1$ μm activated to form cloud droplets varied between 0.34 and 0.74. The cloud droplet r_e ranged between 5 and 8 μm near cloud base to between 6 and 11.5 μm near cloud top; r_e decreased with increasing aerosol loading. The layer-averaged relative dispersion (ε) of the cloud droplet size distribution ranged between 0.2 and 0.8, in all cases decreasing with altitude above cloud-base consistent with droplet growth by uniform condensation. During fixed altitude segments of flights, ε was negatively correlated with both the CDNC and F_a suggesting a dependency between ε and updraft velocity. Comparison of below-cloud CCN spectra to near cloud-base CDNC suggests that the maximum supersaturation achieved during cloud formation was low ($\%SS_{max}$~ 0.05-0.08). The low $\%SS_{max}$ was also consistent with differences between below- and in-cloud accumulation mode particle size distributions. Drizzle water content ($d>50$ μm) was generally low, consistent with the small cloud droplet sizes generally observed in these clouds. The one cloud layer in which significant drizzle was observed exhibited the highest values of r_e, and the smallest CDNC of any of the clouds sampled during the program. Evaluations of newly developed parameterizations for r_e, and for the drizzle threshold function were promising.

1. INTRODUCTION

Extensive sheets of low-lying stratus and stratocumulus clouds are a common feature of the eastern boundary current upwelling regions of the world's oceans. These clouds may exert a large-scale cooling effect on the ocean surface and are an important component of global cloud forcing. Because of their low droplet number concentrations and modest depths, the albedo of marine stratus is thought to be particularly susceptible to additions of aerosols that can act as CCN. Such additions cause an increase in the droplet number concentrations and a decrease in their size, resulting in enhanced short-wave cloud albedo. These aerosol-induced alterations of the albedo in marine stratus clouds are thought to be a major component of the first aerosol indirect effect [*Twomey,* 1977]. Alterations of droplet microphysics by aerosols are also thought to inhibit precipitation formation increasing cloud lifetime and coverage and thereby enhancing the planetary albedo. Indeed, marine stratus are known to have at least two stable modes: one with relatively large cloud droplets and relatively large drizzle rates and another with smaller cloud droplets and little or no drizzle, and aerosol loading is thought to play a critical role in determining which of these two modes is observed [*Baker and Charlson*, 1990]. This inhibition of precipitation by aerosols is known as the second indirect aerosol effect [*Albrecht,* 1989].

A number of studies of the effect of aerosol loading on marine cloud microphysics have been conducted [e.g., *Yum et al..*, 1998; *Chuang et al..,* 2000; *Hudson and Yum,* 2001, 2002; *Yum and Hudson*, 2002; *Snider et al.*, 2003; *Twohy et al.*, 2005]. In general increases in aerosol loading have been found to increase cloud droplet number concentrations and to decrease their size, but the slope of the increase in the cloud droplet number concentration with aerosol loading has differed greatly from study-to-study. Although no definitive explanation for differences in the response of clouds to aerosol loading observed in these various studies has been advanced, it is probable that this results from different cloud dynamics characteristic of the different locations/situations in which these studies were conducted. In nearly all studies it has also been observed that this slope decreases as the aerosol loading increases implying a saturation effect. This saturation effect is likely due to competition between aerosol particles for water vapor during cloud formation at high aerosol loading [*Jensen and Charlson,* 1984]

There have also been reports that the spectral dispersion, ε, of the cloud droplet size distribution (defined as the ratio of the standard deviation of the droplet size distribution to the mean radius) is also affected by aerosol loading [*Hudson and Yum*, 1997]. *Liu and Daum,* [2000] analyzed data from a number of studies of marine clouds and were able to show that the

spectral dispersion in clouds that had been influenced by anthropogenic aerosols was higher than for background clouds that had formed under similar conditions. This increase in ε with aerosol loading has the effect of reducing the magnitude of the first indirect aerosol effect by 10-30% [*Rotstayn and Liu*, 2003]. While there has been some theoretical and modeling work done that establishes a basis for the increase in the spectral dispersion with droplet concentration [*Wood,* 2002; *Feingold and Chuang*, 2002; *Xue and Feingold*, 2004; *Yum and Hudson,* 2005; *Liu et al.,* 2005], all of the factors that determine ε are not well understood.

Observational studies of the second indirect aerosol effect in marine stratus have been sparse no doubt due to the difficulty of documenting the enhanced persistence of clouds associated with alterations of their microphysics by anthropogenic aerosols. What studies there are have focused on the effects of aerosol loading on cloud microphysics, and the effects of cloud microphysics on the formation of drizzle [e.g., *Yum and Hudson,* 2002; *Hudson and Yum*, 2002; *Powlowska and Brenguier*, 2003; *Twohy et al*., 2005]. Generally it has been found that marine stratus that have been strongly influenced by anthropogenic aerosols tend to have very little drizzle in comparison to equivalent background clouds, in qualitative agreement with the second indirect aerosol effect hypothesis. An issue in estimating the magnitude of second indirect aerosol effect using GCM calculations is an accurate and tractable representation of the autoconversion process whereby cloud droplets are converted to drizzle. Recent theoretical advances [*McGraw and Liu*, 2003; 2004] have provided a basis for a more fundamental understanding of the drizzle formation process that subsequently has been applied to the development of a series of parameterizations to represent this process in models [*Liu and Daum*, 2004; *Liu et al*., 2004; *Liu et al.,* 2005, *Liu et al.,* 2006a, *Liu et al*., 2006c].

In this contribution, measurements of aerosol, CCN and cloud macro- and micro-physical properties made aboard the DOE G-1 research aircraft during the 2005 MASE Program that sampled marine stratus clouds off the coast of northern CA during July 2005 are examined. The purpose of the MASE study was to use the low altitude marine stratus/stratocumulus clouds that commonly occur off the coast of Northern California as a natural laboratory to examine the effects of aerosol loading and size distribution on cloud droplet microphysics, and the effects of cloud microphysics on the formation of drizzle. The day-to-day vertical and horizontal variation of cloud microphysical properties including droplet number concentration, size distribution, effective radius and dispersion are examined, and sources of both the vertical and horizontal trends and variability are discussed. The conditions under which drizzle is observed are related

to cloud microphysical properties, and newly developed parameterizations for the effective radius and for the drizzle threshold function are compared to observations.

2. EXPERIMENTAL

The Marine Stratus/Stratocumulus Experiment (MASE) was a collaborative effort between the DOE Atmospheric Sciences Program (ASP), the DOE Atmospheric Radiation Measurements Program (ARM), and the Naval Research Laboratory's Center for Remotely Piloted Vehicles for Atmospheric Studies (CIRPAS). ARM deployed their mobile facility at Pt Reyes National Seashore just North of San Francisco as part of the Marine Stratus Radiation, Aerosol and Drizzle experiment (MASRAD) along with a complement of instrumentation provided by the DOE ASP program. CIRPAS flew a Dehaviland Twin Otter aircraft outfitted with an array of chemical and microphysical instrumentation to measure the aerosol chemistry and aerosol and cloud microphysics; ASP flew the DOE G-1 aircraft. Since we report data here only from the DOE G-1, details of these other platforms will not be discussed further.

The G-1 carried a suite of instrumentation to measure aerosol composition and the microphysical properties of aerosols and clouds, state parameters, winds, and radiation fields. Instrumentation included an Aerodyne quadrapole aerosol mass-spectrometer that measures the non-refractory component of aerosol composition and a particle into liquid sampler (PILS) that measures the soluble inorganic component of the aerosol mass. Cloud condensation nuclei (CCN) concentrations were measured with a Desert Research Institute CCN spectrometer [*Hudson,* 1989] operating over a range of S of 0.02-1%, and two DMT CCN instruments (Droplet Measurement Technologies, Boulder, CO) operating at supersaturations of ~0.08% and 0.2% respectively. Condensation nuclei (CN) particle concentrations of diameter $d > 3$ nm and $d > 10$ nm were measured with a TSI 3025 and a TSI 3010 CN counters respectively. Aerosol number distributions were measured with a Scanning Mobility Particle Sizer (SMPS) that has been described elsewhere *Wang et al.*. [2003]. Aerosol scattering was measured with a TSI three wavelength integrating nephelometer. O_3 was measured with a UV absorption instrument (Thermo Environmental Instruments, Model 49-100) and SO_2 with a modified pulsed fluorescence instrument (Thermo Environmental Instruments, Model 43s). Sample air for these instruments was provided by a low turbulence inlet operated at near isokinetic conditions. Fluid dynamics calculations indicate that the inlet should pass with 50% efficiency, particles that are smaller than 1.5 μm. Cloud droplets impacted on the inlet and fragmented forming much smaller

particles that could be detected by the SMPS system. For this reason DMA and CCN data taken in-cloud were not included in this analysis.

An optical particle probe (PCASP-100X, Particle Metrics Inc., Longmont, CO) mounted on a pylon on the nose of the aircraft measured the size resolved number concentration over the nominal size range $0.1 < D_p < 3$ μm. Measurements were made with probe de-icing on, which resulted in evaporation of most of the water from the ambient aerosol, and we assume in our analysis that size distributions derived from PCASP data represent dry aerosol. There was no evidence of shattering of cloud droplets on the inlet of the PCASP as there was no enhancement in the number concentration of particle concentrations in the smallest size bins of the instrument during the in-cloud segments of these flights. It is presumed that if such shattering occurred that the residual particles were smaller than the nominal 0.1 μm detection limit of the instrument. There was also evidence that some small fraction of the cloud droplets were partially dried during transit through the heated inlet of the PCASP and detected as interstitial aerosol particles as indicated by the presence of a particle mode in the 1-3 μm size range in-cloud that was not present in clear-air. To eliminate this contamination, a size cut of $d<0.5$ μm was used to compute the interstitial aerosol number concentration. Defining interstitial aerosol in this way allowed for a self-consistent apportioning of cloud particles between interstitial aerosol and cloud droplets. Calibration of the probe with polystyrene spheres was performed several times during the field mission. Size bins were adjusted for refractive index assuming an aerosol composition of ammonium sulfate [*Liu and Daum,* 1998].

Cloud and drizzle number concentrations were measured with a Cloud Aerosol and Precipitation Spectrometer (CAPS) (Droplet Measurement Technologies, Boulder, CO). This two-section instrument measures droplets in the 0.5-25 μm diameter range [Cloud Aerosol Spectrometer (CAS) section] using a light scattering technique, and droplets in the 25-1550 μm diameter range using an imaging technique [Cloud Imaging Probe (CIP) section]. The probe was calibrated using precision glass beads and a spinning glass disc with dots of known size at the beginning of the field study. Cloud droplet number concentrations reported below were derived from the CAPS probe, but include only those particles with diameters larger than 1 μm. Drizzle concentrations include particles with diameters greater than 50 μm.

Cloud liquid water content was measured using a Gerber PVM-100 LWC (Gerber Scientific Inc., Reston, VA), the hot wire detector on the CAPS Probe, and by integration of the CAPS probe size distribution from 1-25 μm. (Data from all three probes generally agreed to within about 10%.) The Gerber probe was calibrated using a light-diffusing disk as per the

manufacturers instructions. Liquid water contents discussed in the body of this manuscript are derived from the Gerber Probe measurements.

All G-1 sampling flights originated at Sacramento, CA where the aircraft was based. The flight strategy was to climb to an altitude of ~1.5 km or more after takeoff from Sacramento and head west towards Pt. Reyes. Once at Pt. Reyes, the aircraft first flew an above cloud pattern over the site, and then the same pattern at successively lower altitudes. If possible a below-cloud pattern was made, but unfortunately, cloud-bases were generally so low (< 200 m msl) that few below-cloud passes were made during the entire program. Upon completion of sampling at Pt. Reyes, the aircraft headed offshore, and flew repetitive multi-altitude patterns (about 10-15 min/leg) with legs above cloud, at multiple altitudes in-cloud, and as possible, below cloud. A composite map of the flight tracks for all of the G-1 flights is shown in Figure 1. Dates and locales of flights are given in Table 1. Thirteen flights were made; seven of these flights yielded useful cloud data. The remainder of the flights was either clear-air, broken clouds, or experienced problems that rendered the data unusable.

For the most part, data that will be examined here comes from the multi-altitude legs that were flown offshore; the only exception being the flight on 7/19 which is divided into two segments, 7/19a over Pt Reyes, and 7/19b, offshore. In addition, the offshore flight on 7/20 was divided into two segments because the northeast segment of the flight (designated 7/20a) was clearly conducted in a different air-mass than the southwest segment of the flight (designated 7/20b). Data are presented here mostly as averages and standard deviations of 10s data collected over a flight leg at a given altitude. Since these legs were usually on the order of 10-12 min in length and the aircraft flew at ~100m/s, the data reported and plotted here represent averages on spatial scales of the order of 60-70 km, and standard deviations reflective of variations over a 1 km scale.

3. RESULTS

3.1 Macroscopic cloud properties

Cloud base and top heights, and the sampling altitudes of the G-1 for the clouds examined here are given in Figure 2a; Figure 2b shows the liquid water paths derived from the vertical profiles of liquid water content measured using the Gerber probe. In all cases, clouds sampled during MASE were low-level stratus clouds with cloud thicknesses ranging from about 220 to about 400 m bounded at cloud top by a very strong subsidence inversion (not shown). Cloud bases were generally below 100 m (msl), and frequently appeared to reach the ocean surface;

cloud tops ranged between ~220 and ~450 m (msl). For all of the clouds that were sampled, the layer averaged cloud liquid water content varied linearly from cloud-base to cloud-top. Cloud liquid water paths ranged from about 35 g/m^2 to about 150 g/m^2. With the exception of the flight on 7/15, there was an excellent correlation ($r^2 = 0.94$) between cloud thickness and LWP.

With the exception of the clouds sampled on 7/15 all of these clouds exhibited average liquid water paths that were substantially lower (by as much as 50%) than the liquid water paths computed from the moist adiabatic lapse rate (Table 2). The reason for this is not apparent. Cloudwater could have been removed because of drizzle, but none of the clouds exhibited significant amounts of drizzle as will be shown below. The sub-adiabatic liquid water content may also arise because of entrainment from cloud top, although the rate of such entrainment would be constrained by the strong cloud-top temperature inversion. But it must be remembered that the rate of entrainment is also controlled by the net radiative flux at cloud top, which has a strong diurnal cycle. During the daytime, solar heating just inside the cloud offsets IR cooling, thereby reducing the net cooling at cloud top and attenuating the production of kinetic energy. More vigorous entrainment and mixing are typically observed at night driven by IR cooling and the clouds drizzle more in response to the thickening of the cloud layer. Solar heating during the daytime reduces mixing and disables the influx of vapor from below. Thus, it is possible that the subadiabatic characteristics of these clouds were caused by nocturnal processes, but left a fingerprint that was observed.

3.2 Aerosol Loading

The physical disposition of the clouds sampled during this program made it usually not possible to unambiguously sample pre-cloud or cloud-free air to estimate the aerosol loading. Instead we estimate the aerosol loading (defined here as particle number density, cm^{-3}) as the sum of the interstitial aerosol (IANC) and cloud droplet number concentration (CDNC) considering only particles with sizes > 0.1 μm. The particle number concentration measured by the PCASP probe with d<0.5 μm was used as a measure of the interstitial aerosol, and the number of particles with d >1μm diameter measured by the CAS probe was used as a measure of the aerosol particles that had been activated to form cloud droplets. The sum of the activated and unactivated aerosol particles should represent the loading of particles with d >0.1 μm as long as the maximum supersaturation during cloud formation was not sufficiently high to activate particles with d < 0.1 μm and as long as there is no overlap between particles counted by the PCASP and the CAS. That this is the case is demonstrated in Figure 3 which in panels a-c

respectively, shows time plots of L, CDNC and IANC during a transect through a broken cloud on the flight made on 7/18. As might be expected the CDNC (panel b) is negligible when L is zero, and variable elsewhere. The aerosol concentration varies between a maximum value of ~300-340 cm^{-3} during periods when L is zero, and variable, but lower values when L is finite. Figure 3d shows a scatterplot of the CDNC as a function of the IANC. The data are well correlated with an $r^2 = 0.83$ and a regression slope, assuming errors in both the CDNC and IANC of 0.92 +/- 0.04. Since the errors in both the PCASP and the CAPS probe are on the order of 20%, a slope of this value is consistent with a one-to-one relationship between the decrease in the IANC and the increase in the CDNC, and that the sum is constant, and representative of the aerosol loading to within the uncertainty of the measurements. Profile-averaged accumulation mode particles thus evaluated are shown in Figure 4a. The highest average particle concentration (~620/cm^3) was observed on 7/27 the lowest (~290/cm^3) on 7/19a. Particle concentrations of this magnitude suggest a marine boundary layer that was substantially influenced by anthropogenic emissions, even on the day with the lowest aerosol loading. On most days the aerosol particle loading was either constant as a function of altitude above cloud-base consistent with a well mixed marine boundary layer, or increased by as much as ~10% towards cloud top. An example of the latter is shown in Figure 5. One possible explanation for the increase in the aerosol towards cloud top is entrainment of above cloud air as a layer with very high aerosol concentrations was found trapped in the temperature inversion just above cloud on most days; an example of this is shown in Figure 5. The source of this above-cloud aerosol is not known, but it has been previously reported that it had a composition and CCN activity that was very different from the aerosol measured at lower altitudes [*Alexander et al.,* 2005; *Hudson*, 2007].

3.3 Cloud droplet number concentration and size

Profile averaged cloud droplet number concentrations (CDNC hereafter) shown in Figure 4b varied significantly from day-to-day. The lowest CDNC were observed on 7/19a where mean droplet concentrations were below 100 cm^{-3}, a value usually associated with remote marine air. Droplet concentrations on the remainder of the flights ranged between 180 and 300 cm^{-3}, and were highest at ~350 cm^{-3} on 7/27. These latter values are characteristic of stratus/stratocumulus cloud droplet concentrations found in a moderately polluted boundary layer. On many flights the layer-average CDNC increased with altitude above cloud-base; examples are shown in Figure 6; similar behavior has been observed in previous studies [*Miles et al.,* 2000]. The reason for the

vertical gradient in the CDNC is not clear. It could be that towards cloud-top where liquid water contents are high additional aerosol particles grow into the size range of cloud droplets. This seems a reasonable explanation, but seems inconsistent with the concurrent growth in aerosol concentration with altitude that was observed on many of these same days. Another possible explanation is entrainment of aerosol from just above cloud top, but there seems to be no mechanism for activating these particles to form cloud droplets as any increased water vapor induced, for example, by turbulence, would be taken up by existing cloud droplets. Vertical gradients in the CDNC could also be caused by drizzle that is typically initiated towards cloud top and progressively depletes cloud droplets by collision when falling through the cloud towards cloud-base. But as will be shown below, only a few of these clouds exhibited significant concentrations of drizzle. So the observed vertical gradient in droplet concentrations has no ready explanation. Significant variability in the cloud droplet concentration at constant altitude was observed on all flights. The source of this variability will be addressed below.

The cloud droplet effective radius, r_e, was computed from the size distributions measured by the CAPS probe. Mean values for individual flights are shown in Figure 4c and it should be noted that there was nearly a factor of two difference between clouds exhibiting the lowest mean value of the effective radius (5.8 μm) and the highest (10.3 μm). On individual flights r_e always increased with altitude, consistent with droplet growth by condensation of water due to the decrease in temperature. Significant variations in the effective radius were observed during constant altitude portions of the flights. These variations were negatively correlated with CDNC. The observed values of r_e are within the range of values reported for a combination of continental and marine stratus/stratocumulus clouds in *Miles et al.* [2000] and with values recently reported for marine stratocumulus clouds off the CA coast south of the region sampled during MASE [*Twohy et al.*, 2005].

3.4 The fraction of particles activated to form cloud droplets

The fraction of accumulation mode particles activated to form cloud droplets, F_a, is estimated as the ratio of the CDNC to the sum of the interstitial aerosol ($0.1<d<0.5$ μm) and the CDNC. Flight averaged values of F_a (Figure 4d) exhibited significant day-to-day differences with a low of ~0.34 and a high of ~0.74. There was no statistically significant correlation between flight averaged values of F_a and the aerosol loading as defined above ($r^2 = 0.0003$), suggesting that the fraction of particles activated was independent of the loading and that dynamics was the dominant factor in determining the fraction of particles that were activated to

form cloud droplets. In this view, variations in the mean updraft velocity prevailing on a given day leads to variations in the mean $\%SS_{max}$, and this in turn leads to differences in the mean fraction of particles that were activated to form cloud droplets. Thus, clouds with higher values of F_a were formed under conditions where a higher $\%SS_{max}$ was achieved than clouds exhibiting lower values of F_a. This presumes that the properties of the pre-cloud aerosol such as the size distribution, and/or the CCN properties were similar from day-to-day. The cloud layer (7/19a) exhibiting the lowest value of F_a had the lowest CDNC of any cloud sampled during the entire program. This suggests that cloud microphysical properties (number concentration and size) may be more influenced by cloud dynamics (which determines $\%SS_{max}$, and thus F_a), than by aerosol loading and properties. The role of dynamics in determining F_a and hence the CDNC is emphasized by the generally positive relationship between these two quantities during constant altitude flight segments under conditions where aerosol loading was relatively constant.

3.5 CCN spectra, $\%SS_{max}$, and D_{pc}

The relation between the below-cloud CCN spectra, and the CDNC is examined for the purpose of estimating the $\%SS_{max}$ achieved during cloud formation, the minimum sized particles, D_{pc}, that had been activated to form cloud droplets. We restrict our consideration to data collected on 7/19 and 7/20a, because these were among the few flights in which we were able to measure a below cloud CCN spectrum that could be directly connected to cloud microphysical measurements made just above cloud-base. Cumulative below cloud CCN spectra for flights on 7/19a and 7/20a are shown in Figure 7a. These spectra consist of averages of all droplet-free spectra measured during the below-cloud portions of each of these flights. Also shown in the plots is the average CDNC measured just above cloud base. Since there is a 1:1 relationship between the CDNC and the number of CCN that have been activated, $\%SS_{max}$ can be estimated from CCN spectra as shown. $\%SS_{max}$ for the 7/19a and the 7/20 flights were 0.055% and 0.069% respectively. These low $\%SS_{max}$ values suggest that these clouds formed under conditions where updraft velocities were very low.

Since we also have below-cloud aerosol size distributions, D_{pc} of dry particles that were activated to form cloud droplets can also be estimated; for the 7/19a flight the minimum size is 0.18 μm, and for the 7/20a flight, 0.21 μm (Figures 7b). This estimate assumes that the aerosol particles were internally mixed. If for example, the pre-cloud aerosol consisted of an external mixture of refractory materials and ammonium sulfate the estimated $\%SS_{max}$ would be higher, and the estimated D_{pc} would be lower. But, activation curves for different substances suggest

that these particles were ammonium sulfate-like in their CCN behavior (ammonium sulfate particles of 0.18 μm diameter activate at a supersaturation of ~0.06%, and 0.21 diameter particles at 0.05%, reasonably consistent with the data in Figures 7a and 7b), so we believe that estimates of D_{pc} are reasonably robust.

3.5 Dispersion of the droplet size distribution

With the exception of flight 7/20a, the average relative dispersion of the cloud droplet size distribution, ε, varied within a relatively small range of (0.32-0.45) of values (Figure 4e). These values are comparable to those reported for marine and continental clouds, of 0.395 and 0.483 respectively, by *Miles et al*. [2000]. In contrast to many previous observations [*Miles et al*.., 2000], ε decreased with altitude in nearly all of the clouds that were sampled during the program. An example of this altitude dependency is shown in Figure 8. The decrease in dispersion with altitude is expected since the growth of a population of droplets by condensation processes as they rise through a cloud will cause the droplet size distribution to narrow because the relative growth of the smaller droplets will be faster than the growth of the larger particles, but this is not always observed [*Rogers and Yau*, 1989; *Nicholls and Leighton*, 1986; *Martin et al.,* 1994].

Although the profile-averaged values of ε did not vary substantially among flights, a significant variation in ε was found on all days when flying at a constant altitude as indicated by the spread of points in Figure 8. During these constant altitude legs, ε was always found to be negatively correlated with the CDNC, and with F_a; Figure 9 gives an example from the 7/27/05 flight. Since for this example, and in general, neither ε nor the CDNC were well correlated with the accumulation mode aerosol number concentration ($r^2 = 0.040$ for the ε-aerosol loading correlation and 0.006 for the CDNC- aerosol loading correlation for the data in Figure 9), variables other than aerosol loading must be responsible for this systematic trend in ε with the CDNC. The negative dependency of ε on both the CDNC and F_a indicated in Figures 9a and 9b suggests that variations in updraft velocity causing variations in $\%SS_{max}$ are responsible for the negative correlation between ε and the CDNC. This decrease in ε with increasing CDNC is consistent with both adiabatic parcel model concentrations that predict a decrease in ε with updraft velocity at fixed aerosol loading, and with predictions from a recently developed parameterization for ε [*Liu et al*., 2006b].

The relationships expressed above might be considered counter to the concept of "dispersion warming' [*Liu and Daum,* 2002] wherein increasing aerosol loading causes an

increase in the relative dispersion of the droplet size distribution, leading to a warming effect. But, the data given here neither support nor reject the influence of aerosol loading on the spectral dispersion of the droplet size distribution. What is presented here indicates that there are a number of factors that determine the spectral dispersion of the droplet size distribution including turbulence, and updraft velocity, in addition to aerosol loading.

3.6 Drizzle

All clouds sampled during the program had some drizzle (defined here as droplets with d> 50 μm), but day-to-day amounts differed by nearly a factor of 20. The highest average drizzle concentrations were observed on the flight of 7/19a and the lowest amounts on the flights of 7/15 and 7/27 (Figure 4f). Not coincidentally, the clouds sampled during the 7/19 flight contained the largest-sized cloud droplets observed during the entire program and those sampled on the 7/15 and 7/27, the smallest (Figure 4c). For all clouds sampled, the drizzle water content increased from cloud-top to cloud-base, as did the size of the drizzle droplets, similar to observations made previously [*Hudson and Yum*, 1997]. Examples are shown in Figure 10 for clouds exhibiting the highest (7/19), and the lowest (7/27) drizzle water content. The vertical trend in drizzle water content and size is consistent with initiation of drizzle near cloud top where cloud droplet size and liquid water content are the highest, and growth of these newly formed drizzle drops by a collision-coalescence process as the droplets fall from cloud top towards cloud base. Note that the trend of drizzle properties with altitude are opposite to the trend exhibited by cloud droplets in that the cloud droplet liquid water content, and the cloud droplet effective radius are lowest at cloud base, and increase nearly monotonically towards cloud top.

An example of the suppression of drizzle by an enhancement in the aerosol loading is shown in Figure 11 for a flight made in the vicinity of Pt Reyes on 7/19a. The cloud liquid water content and the interstitial aerosol number concentration shown in Figure 11a indicate an encounter with a substantial aerosol plume at about 17:05 that increased the interstitial aerosol concentration by approximately a factor of 2. This increase in the interstitial aerosol concentration was associated with, an increase in the cloud droplet concentration by nearly a factor of 5 (Figure 11b), and a decrease in the cloud droplet effective radius from between 10 and 12 μm to about 6 μm. Associated with this change in cloud properties was a nearly complete suppression of the drizzle concentration (Figure 11c).

3.7 Dispersion and parameterization of the r_e

Parameterization of r_e for purposes of computing cloud radiative properties is frequently done in terms of the prognostic variables L and N, viz.,

$$r_e = 3/(4\pi\rho_w)\beta(L/N)^{1/3} = \beta_{rv} \ . \qquad (1)$$

where ρ_w is the density of water, L, the cloud liquid water content, N the droplet concentration, r_v, the volume mean radius, and β is a dimensionless parameter that depends on the spectral shape of the cloud droplet size distribution. It is commonly assumed that β is either a constant or varies as a function of cloud-type. For example, *Martin et al*. [1994] assumed that β was 1.08 for maritime and 1.14 for continental stratocumulus clouds. Recently it has been shown [*Liu and Daum*, 2000] that β is a function of ε and that for a gamma droplet size distribution, the dependency of β on ε takes the form,

$$\beta = (1 + 2\varepsilon^2)^{2/3}/(1 + \varepsilon^2)^{1/3}. \qquad (2)$$

A test of this parameterization is to compare the effective radius computed from the measured size distribution to that computed from Eqs. 1 and 2 using measured values of L, N and ε. Such a comparison is shown in Figure 12. The values of r_e computed assuming a constant value of β (a value 1.18 which is the mean value of β for all measurements included in our analysis) is also shown to illustrate the effects of assuming a constant value of ε. Regression analysis between r_e computed from the new parameterization and measured values of r_e had a slope and intercept of 0.996 and -0.14 respectively, and an r^2 of 0.92; for the parameterization that does not include ε, the slope, intercept and r^2 values are 0.945, 0.33 and 0.67 respectively. Figure 12 clearly shows that accounting for the values of ε through Eq. 2 greatly improves the parameterization of r_e in comparison to assuming a fixed value for ε and thus β. The issue then becomes how to parameterize ε in terms of readily predictable variables.

3.8 Parameterization of the drizzle threshold function.

In Section 3.6 we qualitatively examined the effect of the CDNC and size on the presence of drizzle. Here, we take the opportunity to examine a new parameterization for the drizzle threshold function in the context of the microphysical properties of clouds observed during this

program, and the measured drizzle concentration. The rate of formation of drizzle water P ($g/(m^3 sec)$, is usually represented as the product of a rate function, P_0, and a threshold function T, viz.,

$$P = P_0 T. \quad (3)$$

where T varies between 0 and 1. Various ways of specifying T have been developed over the years (for a discussion see *Liu et al.,* [2004]), the simplest of which is to assume that T is a Heaviside step function that according to variously specified criteria, transitions abruptly from 0-1. Recently we have developed a parameterization for T, denoted T_{LDM} (LDM for Liu, Daum, McGraw) based upon kinetic potential theory of droplet formation that is testable with the data collected during this study [*Liu et al.,* 2006]. T_{LDM} takes the form,

$$T_{LDM} = 1/2(X_c^2 + 2 X_c + 2)(1 + X_c)\exp(-2 X_c), \quad (4)$$

where

$$X_c = 9.7 \times 10^{-17} N^{3/2} L^{-2}, \quad (5)$$

and N and L are the cloud droplet number concentration and liquid water content respectively. X_c is defined as the ratio of the critical to the mean droplet mass. If $X_c << 1$, $T_{LDM} = 1$, $P=P_0$ and the cloud drizzles; if $X_c >> 1$, P=0 and the cloud does not drizzle; when $T_{LDM} = 0.5$, $1/ X_c \sim 0.72$.

Values of T_{LDM} averaged over the highest in-cloud altitude sampled on each of the flights are superimposed on the plot of the profile-averaged drizzle water content (Figure 4f). With the exception of the 7/15 flight, there is a reasonable relationship between drizzle water content and the value of T_{LDM}. T_{LDM} is highest on 7/19a, the flight that exhibited the highest mean drizzle water content, and is quite low on the very low drizzle days, 7/16, 7/17 and 7/28. It is not clear why 7/15 is anomalous, but there may have been a sampling problem in that the in-cloud leg used to estimate T_{LDM} was not coincident geographically with the in-cloud legs used to estimate the drizzle water content

It is interesting to examine the behavior of T_{LDM} as a function of altitude above cloud base. Shown in Figure 13 are vertical profiles of T_{LDM} computed from data collected during vertical sampling conducted on 7/19a, and 7/27 high- and low-drizzle flights respectively. In both cases T_{LDM} increases with altitude above cloud-base. Since N only changes by ~10-20% from cloud-base to cloud-top, the increase in T_{LDM} is attributed to increases in L with altitude. The central point of Figure 13 is that drizzle is not uniformly initiated throughout the cloud, but is formed

preferentially towards cloud-top where L is the highest. How high L needs to be (or how thick the cloud needs to be) before drizzle is initiated depends on the number of cloud droplets. On the low drizzle day where the droplet concentrations are a factor of 3 or so higher than on the high drizzle day, the cloud would need to be considerably deeper than it is for drizzle to be formed.

The response of T_{LDM} to variations in cloud microphysics during level flight is shown in Figure 11c. As discussed above, an aerosol plume imbedded in a cloud layer sampled on 7/19a caused an increase in the cloud droplet concentration, a decrease in r_e, and a suppression of the drizzle number concentration. In Figure 11c, it may be seen that T_{LDM} is highly correlated with the drizzle water concentration: in the region outside of the aerosol plume, T_{LDM} is on the order of 0.8 and the drizzle droplet concentration is 0.03-0.04 cm^{-3}; in the aerosol plume T_{LDM} decreases to near zero, and the drizzle concentration decreases to about 0.005 cm^{-3}, a factor of 7 to 8 below concentrations outside of the plume.

3.9 Evidence for the first and second indirect aerosol effects

Aerosol loading and the first indirect aerosol effect. Here we explore the relationship between CDNC and size, and between aerosol loading and CDNC and size. The mean value of the effective radius measured on a given flight, was found to be a strongly decreasing function of the corresponding mean value of the cloud droplet number concentration (Figure 14a). There is also a reasonably robust relationship between the mean aerosol loading and the mean CDNC (Figure 14b). As expected the CDNC increases with aerosol loading, and is well described by a linear relationship, but the slope is only 0.5 indicating that there is not a 1:1 relationship between increases in aerosol loading and increases in the CDNC. In interpretation of Figure 14b however, it should be recognized that the aerosol loading and the CDNC are not truly independent since the CDNC was used in the calculation of aerosol loading as explained in 3.2. Figure 14c shows that as the aerosol loading increases the mean r_e decreases; for these data when the aerosol loading increases by a factor of two (300-600 cm^{-3}), r_e decreases by nearly a factor of two (10.3-5.8). The responses of the CDNC and r_e to an increase in the aerosol loading are an example of the Twomey effect, but the relationships are noisy. The noisiness is not surprising considering that the fraction of accumulation mode particles activated to form cloud droplets varied from day to day (Figure 4d) suggesting that droplet microphysics are determined as much by the conditions prevailing during cloud formation as by the aerosol concentration itself, an

important factor to remember when examining experimental data regarding the Twomey effect. Noise in the relationship between r_e and CDNC can also be induced by day-to-day variations in cloud depth (Figure 2a) since all other factors being equal, deeper clouds will have larger droplets than shallow clouds. In fact the only reason that the relationships shown in Figure 14 are as good as they are, is that the clouds sampled here had very similar depths and liquid water contents.

Drizzle and the second indirect aerosol effect. The dependency of drizzle water content on the effective radius of the cloud droplet size distribution is shown in Figure 15a where we have plotted the average drizzle concentrations measured during vertical profiles conducted during the various flights against the average values of the cloud droplet r_e. As expected from theories of drizzle formation, the drizzle water content increases steeply as the effective radius increases. The inverse dependency of the drizzle water content on the CDNC is shown in Figure 15b. Such behavior is central to the "second indirect aerosol effect" wherein increased aerosol loading causes an increase in the CDNC, a decrease in droplet size, and a consequent decrease in the drizzle concentration. However, as shown in Figure 15c, the relationship between the drizzle water content and the aerosol loading is not nearly as strong as the relationship between the drizzle water content and the CDNC. This emphasizes that there are number of quantities other than aerosol loading that determine the number of aerosol particles that get activated to form cloud droplets, and the size that they achieve. These quantities include the number of aerosol particles, the fraction of particles that get activated, which is determined by $\%SS_{max}$, which in turn is determined by the updraft velocity, cloud depth, which determines how large a population of particles will grow, and by dynamical factors such as turbulence and entrainment.

4. SUMMARY AND CONCLUSIONS

Properties of marine stratus/stratocumulus clouds were measured over the Eastern Pacific Ocean on seven days during the month of July 2005. These clouds were low-level stratus with cloud thicknesses ranging from about 200 to about 400 m. Cloud bases were generally below 100 m (msl) and frequently appeared to reach the ocean surface. In all cases cloud top was associated with a strong temperature inversion that inhibited mixing with air from aloft. Cloud liquid water content increased nearly linearly from cloud base to cloud top in all of the clouds, but on six of the seven cloud flights, the liquid water path was sub-adiabatic. Average accumulation mode aerosol particle loading measured during these flights ranged between ~300

cm^{-3} and ~600 cm^{-3}, suggesting a significant anthropogenic contribution to the aerosol loading even on the flight exhibiting the lowest aerosol concentration. A layer of enhanced aerosol concentration just above cloud top was observed on nearly all flights. Average CDNC ranged between ~100 cm^{-3} and 350 cm^{-3}. On many flights the CDNC increased with altitude above cloud base, but the cause of this is uncertain.

Comparison of below-cloud CCN spectra to near cloud-base CDNC suggests that the maximum supersaturation achieved during cloud formation was generally low ($\%SS_{max}$~0.05-0.08). This is consistent with the values of F_a, which ranged between 0.34 and 0.74. There was a strong relationship between the CDNC and F_a suggesting that dynamics was an important factor in determining the fraction of aerosol particles that were activated to form cloud droplets. The cloud droplet r_e increased with altitude above cloud base on all of the flights ranging between 5 and 8 μm near cloud base to between 6 and 11.5 μm near cloud top. The layer-averaged values of ε ranged between 0.2 and 0.8, in all cases decreasing with altitude above cloud-base. The vertical gradient in both the r_e and ε is consistent with droplet growth by uniform condensation as the temperature decreases with altitude. On a given flight at constant altitude, ε was negatively correlated with both the CDNC and F_a suggesting a relationship between ε and updraft velocity. A new parameterization for r_e in terms of L, N_{cd} and ε, was compared to values of r_e computed from the measured droplet size distribution, and to a parameterization for r_e that assumes ε is constant. This comparison clearly indicates the need to include the effects of shape of the droplet size distribution in the parameterization of r_e.

Drizzle water content (d>50 μm) was generally low consistent with the small cloud droplet sizes generally observed in these clouds. The one cloud layer in which significant drizzle was observed exhibited the largest cloud droplet sizes, and the smallest CDNC of any of the clouds sampled during the program, consistent with our understanding of the microphysical processes associated with drizzle formation. A new parameterization for the threshold function for drizzle initiation was examined in the context of the measured drizzle water content. With the exception of one flight, the value of the threshold function was low when the drizzle water content was low and high when drizzle water was high, suggesting that this parameterization has captured the essence of the drizzle formation process. But, since the range of cloud microphysics encountered during MASE was so limited, full evaluation of this parameterization over a relevant range of conditions remains to be completed.

5. ACKNOWLEGEMENTS

The authors thank R V. Hannigan Chief Pilot of the DOE G-1 aircraft for outstanding performance, and S. R. Springston who reduced the aircraft data to a form such that it could be readily analyzed. The Atmospheric Sciences and the Atmospheric Radiation Measurements Program of the US Department of Energy supported this research. The US government retains, and the publisher by accepting this article for publication acknowledges a worldwide license to publish or reproduce the published form of this manuscript, or to allow others to do so, for US government purposes.

6. REFERENCES

Albrecht, B. A. (1989), Aerosols microphysics, and fractional cloudiness, *Science, 245*, 1227-1230.

Alexander et al. (2005), Observations of enhanced organic aerosol concentrations above cloudtops in Marine Stratus Experiment off the Northern California Coast. *Eos Trans. AGU, 86(52) Fall Meet. Suppl.* Abstract A13B-0924.

Baker, M. B. and R. J. Charlson (1990), Bistability of CCN concentrations and thermodynamics in the cloud-topped boundary layer, *Nature, 345*, 142-145.

Chuang, P. Y., D. R. Collins, H. Pawlowska, J. R. Snider, H. H. Jonsson, J. L. Brenguier, R. Flagan, and J. Seinfeld (2000), CCN measurements during ACE-2 and their relationship to cloud microphysical properties, *Tellus, 52B*, 843-867.

Gerber, H. (1996), Microphysics of marine stratocumulus clouds with two drizzle modes, J. Atmos. Science, *53,* 1649-1662.

Hudson, J. G. (1989), An instantaneous CCN spectrometer, *J. Atmos. Oceanic Technol., 6*, 1055-1065 .

Hudson, J.G. and S.S. Yum (1997), Droplet spectral broadening in marine stratus. *J. Atmos. Sci., 54*, 2642-2654.

Hudson, J. G., and S. S. Yum (2001), Maritime-Continental drizzle contrasts in small cumuli, *J. Atmos. Sci.,* 915-926.

Hudson, J.G., and S.S. Yum (2002), Cloud condensation nuclei spectra and polluted and clean clouds over the Indian Ocean. *J. Geophys. Res., 107(D19), 8022,* doi:10.1029/2001JD000829.

Hudson, J.G., (2007), Variability of the relationship between particle size and cloud-nucleating ability. *Geophys. Res. Let.*, in press.

Jensen J. and R. Charlson (1984), On the efficiency of nucleation scavenging, *Tellus, Ser. B, 36*, 367-75.

Leaitch, W. R., C.M. Banic, G. A., Isaac, J. M. D. Couture, P. S. K. Liu, I. Gutelpe, S.-M. Li, L. Kleinman, P. H. Daum, and J. I., McPherson (1996), Physical and chemical observations in marine stratus during the 1993 North Atlantic Regional Experiment: Factors controlling cloud droplet number concentrations, *J. Geophys. Res., 101*, 29,123-29,135.

Liu, Y., and P. H. Daum (2000a), Spectral dispersion of cloud droplet size distributions and the parameterization of cloud droplet effective radius. *Geophy. Res. Lett. 27,* 1903-1906.

Liu, Y., and P. H. Daum (2000b), Which size distribution function to use for studies related to effective radius. *13th International Conf. on Clouds and Precipitation, Reno, USA.*

Liu, Y., and P. H. Daum (2002), Warming effect from dispersion forcing. *Nature*, *419*, 580-581.

Liu, Y., and P. H. Daum (2004), Parameterization of the autoconversion process. Part I: Analytical formulation of the Kessler-type parameterizations. *J. Atmos. Sci, 61,* 1539-1548.

Liu, Y., P. H. Daum, and R. McGraw (2004), A new analytical expression for predicting the critical radius in the autoconversion parameterization. *Geophys. Res. Lett.*, *31,* L06121, doi:10.1029/2003GL019117.

Liu, Y., P. H. Daum, and R. McGraw (2005), Size Truncation Effect, Threshold Behavior, and a New Type of Autoconversion Parameterization. *Geophys. Res. Lett. 32,* L11811, doi:10.1029/2005GL022636.

Liu, Y., P. H. Daum, R. McGraw, and R Wood (2006a), Parameterization of the autoconversion process. Part II: Generalization of Sundqvist-type parameterizations. *J. Atmos. Sci. 63*, 1103-1109.

Liu, Y., P. H. Daum, and S. Yum (2006b), An analytical expression for predicting relative dispersion of the droplet size distribution. *Geophys. Res. Lett, 33*, l02810, doi10.1029/2005GL024502.

Liu, Y., P. H. Daum, R. McGraw and M. Miller (2006c), Generalized threshold function accounting for the effect of relative dispersion on threshold behavior of autoconversion process. *Geophys. Res. Lett, 33*, L11804, doi:10.1029/2005GL025500.

Lohmann, U., and J. Feichter (2001), Can the direct and semi-direct aerosol effect compete with the indirect effect on a global scale? *Geophys. Res. Lett*, *28 (1)*, 159-161.

Martin, G.M., D.W. Johnson, and A. Spice, (1994), The measurement and parameterization of effective radius of droplets in warm stratocumulus clouds. *J. Atmos. Sci.*, *51*, 1823-1842.

McGraw, R. and Y. Liu (2003), Kinetic potential and barrier crossings: A model for warm cloud drizzle formation. *Phys. Rev. Lett.*, *90(1)*, 018501-1 - 018501-4.

McGraw, R. and Y. Liu (2004), Analytical formulation and parameterization of the kinetic potential theory for drizzle formation. *Phys. Rev. E. 70*, 031606-1-13.

McGraw, R. and Y. Liu, Brownian drift-diffusion model for evolution of droplet size distributions in turbulent clouds (2006). *Geophys. Res. Lett., 33*, 103832, doi:10.1029/2005GL1023545.

Miles, N., J. Verlinde, and E. Clothiaux (2000), cloud droplet size distributions in low-level stratiform clouds, *J. Atmos. Sci., 57*, 295-311.

Nicholls, S., and J. Leighton (1986), An observational study of the structure of stratiform cloud sheets. Part I: Structure. *Quart. J. Roy. Meteor. Soc.*, *112*, 431-460.

Pawlowska, H and J-L Brenguier (2003), An observational study of drizzle formation in stratocumulus clouds for general circulation model (GCM) parameterizations, *J. Geophys. Res. 108, D15*, 8630, doi10.1029/2002JD0026799.

Peng, Y. R., and U. Lohmann (2003), Sensitivity study of the spectral dispersion of the cloud droplet size distribution on the indirect aerosol effect. *Geophys. Res. Lett*, *30* (10), Art. No. 1507.

Rogers, R.R., and M.K. Yau (1989), A Short Course in Cloud Physics. Pergamon Press, 393 pp.

Rotstayn, L. D., and Y. Liu (2003), Sensitivity of the first indirect aerosol effect to an increase of cloud droplet spectral dispersion with droplet number concentration. *J. Climate*, *16*, 3476-3481.

Rotstayn, L. D., and Y. Liu (2005), A smaller global estimate of the second indirect aerosol effect. *Geophys. Res. Lett.*, *32*, L05708-1-4.

Rotstayn, L. D., and Y. Liu (2003), Sensitivity of the indirect aerosol effect to the parameterization of cloud droplet spectral dispersion. *J. Climate, 16*, 3476-3481.

Snider, J., S. Guibert, J-L Brenguier, J.-P Putaud (2003), Aerosol activation in marine stratocumulus clouds: 2. Köhler and parcel theory closure studies, *J. Geophys. Res., 108, NO. D15*, 8629, doi:10.1029/2002JD002692.

Twohy, C., M. Petters, J. Snyder, B. Stevens, W. Tahnk, M. Wetzel, L. Russell, F. Burnet (2005), Evaluation of the aerosol indirect effect in marine stratocumulus clouds: Droplet number, size, liquid water path, and radiative impact., *J. Geophys. Res, 110*, D08203, doi:10.1029/2004JD005116.

Twomey, S. (1997), The influence of pollution on the shortwave albedo of clouds., *J. Atmos. Sci.*, *34*, 1149-1152.

VanReken, T., T. Rissman, G. Roberts, V. Varutbangkul, H. Jonsson, R. Flagan, J. Seinfeld (2003), Toward aerosol/cloud condensation nuclei (CCN) closure during CRYSTAL-FACE, *J. Geophys. Res., 108, NO. D20*, 4633, doi:10.1029/2003JD003582.

Yum, S. S., J. G. Hudson, Y. H. Xie (1998), Comparison of cloud microphysics with cloud condensation nuclei spectra over the summertime Southern Ocean. *J. Geophys. Res., 103*, 16625-16636.

Yum, S. S., and J. G. Hudson (2001), Microphysical relationships in warm clouds, *Atmos. Res., 57*, 81-104.

Yum, S. S., and J. G. Hudson (2002), maritime/continental microphysical contrasts in stratus, *Tellus, 54B*, 61-73.

Yum, S. S., and J. G. Hudson (2001), Vertical distributions of cloud condensation nuclei spectra over the springtime Arctic Ocean, *J. Geophys. Res., 109*, D18204, doi:10.1029/2004JD004750.

Yum, S.S., and J.G. Hudson (2005), Adiabatic predictions and observations of cloud droplet spectral broadness. *Atmospheric Research.*, *73*, 203-223.

Wood, R., Parameterization of the effect of drizzle upon the droplet effective radius in stratocumulus clouds (2000), *Quart. J. Royal Meteor. Soc.*, 126, 3309-3324.

Wood, R., How important is the spectral ripening effect in stratiform boundary layer clouds? Studies using simple trajectory analysis (2002), *J. Atmos. Sci., 59*. 2681-2693.

Xue, H. and G. Feingold, A modeling study of the effect of nitric acid on cloud properties (2004), *J. Geophys. Res, 109*, D18204, doi:10.1029/2004JD004750.

Table 1. List of flights conducted by the G-1 during the MASE program

Date	Description
7/5/05	Test flight over Pt. Reyes
7/6/05	Joint flight with Twin Otter over Pt. Reyes
7/12/05	Pt. Reyes then due west over Pacific Ocean
7/15/05*	Pt. Reyes then joint flight with Twin Otter west of Monterey
7/16/05*	Pt. Reyes then joint flight with Twin Otter west of Monterey
7/17/05*	Pt. Reyes then west of Monterey
7/18/05*	Pt. Reyes then west of Monterey
7/19/05*	Pt. Reyes then due west over Pacific Ocean
7/20/05*	Pt. Reyes then due west over Pacific Ocean
7/22/05	Pt. Reyes then due west over Pacific Ocean
7/23/05	Pt. Reyes then due west over Pacific Ocean
7/25/05	Pt. Reyes then due west over Pacific Ocean
7/27/05	Pt. Reyes then due west over Pacific Ocean

*Flight yielded interpretable cloud data

Table 2. Comparison of observed to adiabatic LWP

Date	Cloud-base T[1] ^{o}C	Adiabatic LWP[2] (g/m^2)	Observed LWP[3] (g/m^2)
7/15	12.3	116	147
7/16	12.0	125	96
7/17	13.0	55	41
7/18	14.3	215	149
7/19a	13.5	202	134
7/19b	13.5	218	126
7/20a	13.0	102	69
7/20b	13.0	110	67
7/27	12.2	190	136

[1] Estimated by extrapolation in cases where G-1 was unable to fly below cloud.

[2] Computed from cloud base temperature using the formulation of Albrecht et al.

[3] Computed from the observed slope of LWP vs altitude.

FIGURE CAPTIONS

Figure 1. Composite Flight track of all G-1 flights conducted during the 2005 MASE Program. Red coloring indicate areas of high population density.

Figure 2a. Cloud vertical extent and G-1 flight sampling altitudes. Vertical extent of clouds indicated by the shaded bar; sampling altitudes by the horizontal lines. b. Cloud liquid water path determined from integration of observed cloud liquid water content.

Figure 3. Measurements of cloud properties measured on 7/18 near cloud base in broken clouds. a. Cloud liquid water content. b. Cloud droplet number concentration. c. Concentration of aerosols with $d < 0.5\ \mu m$. d. Regression plot of CDNC versus concurrently measured aerosol concentration.

Figure 4. Composite properties of clouds sampled by the G-1 during MASE. Symbols represent quantities averaged over all altitudes flown on the indicated flights. Bars represent standard deviations of the indicated quantities. Points in 4f have been offset for clarity.

Figure 5. Vertical profile of cloud liquid water content and total particle concentration measured on a flight conducted on 7/27/05 showing the presence of an aerosol layer just above cloud top. Note also the possible entrainment of aerosol into cloud top at an altitude just less than 400 m.

Figure 6. Vertical profiles of cloud droplet number concentration showing an increase in the droplet concentration with height. Black symbols are 10 s averages, red symbols are layer averages. a. Fight of 7/27/05; b. Fight of 7/16/05.

Figure 7. a. Average below cloud supersaturation spectra for the 7/19/05a, and 7/20/05a flights. The observed cloud droplet concentration is the mean value measured just above cloud-base; lines are power-law fits to the data. b. Below cloud cumulative aerosol size distribution for 7/19/05a and 7/20/05a. The average cloud droplet number concentration measured just above cloud base is used to estimate the minimum size particles that had been activated to form cloud droplets.

Figure 8. Dispersion of the cloud droplet size distribution for the flight made on 7/16/05. Black symbols are 10 s averages. Red symbols are layer averages.

Figure 9. Relative dispersion as a function of a. the measured CDNC for a fixed, and, b. the fraction of particles activated to form cloud droplets for a fixed altitude transect on the flight of 7/27/05.

Figure 10. Drizzle properties for flights exhibiting high and low drizzle concentrations. a. Drizzle water content as a function of altitude, and b. Effective drizzle droplet size as a function of altitude for days exhibiting high and low drizzle concentrations.

Figure 11. Example of the suppression of drizzle by an aerosol plume encountered on the flight of 7/19/05a over Pt. Reyes. a. Time plot of L and accumulation mode aerosol concentration showing the presence of an aerosol plume at 17:07. b. Time plot of r_e and CDNC showing coincident with the aerosol plume an increase in CDNC and a decrease in r_e. c. Time plot of drizzle water concentration and the threshold function, $T_{LDM,}$ for drizzle formation (see text for details) showing a decrease in the number of drizzle droplets and a decrease in the threshold function coincident with the aerosol plume.

Figure 12. Comparison of r_e computed from measurements of the cloud droplet size distribution to r_e computed from $r_e = 3/(4\pi\rho_w)\beta(L/N)^{1/3}$. a. Assuming $\beta = 1.18$, and b. Accounting for the dispersion of the droplet size distribution assuming $\beta = (1 + 2\varepsilon^2)^{2/3}/(1 + \varepsilon^2)^{1/3}$. See text for details.

Figure 13. Comparison of the vertical variation in T_{LDM} for a high drizzle day, and a low drizzle day.

Figure 14. a. Flight averaged r_e as a function of flight averaged CDNC; b. Flight averaged values of the CDNC as a function of aerosol loading; c. r_e as a function of aerosol loading; d. CDNC as function of F_a. Vertical and horizontal bars represent flight-averaged standard deviations.

Figure 15. Average drizzle water content as a function of- a. r_e of the cloud droplet size distribution, b. the CDNC; and, c. aerosol loading. Vertical and horizontal bars represent flight-averaged standard deviations.

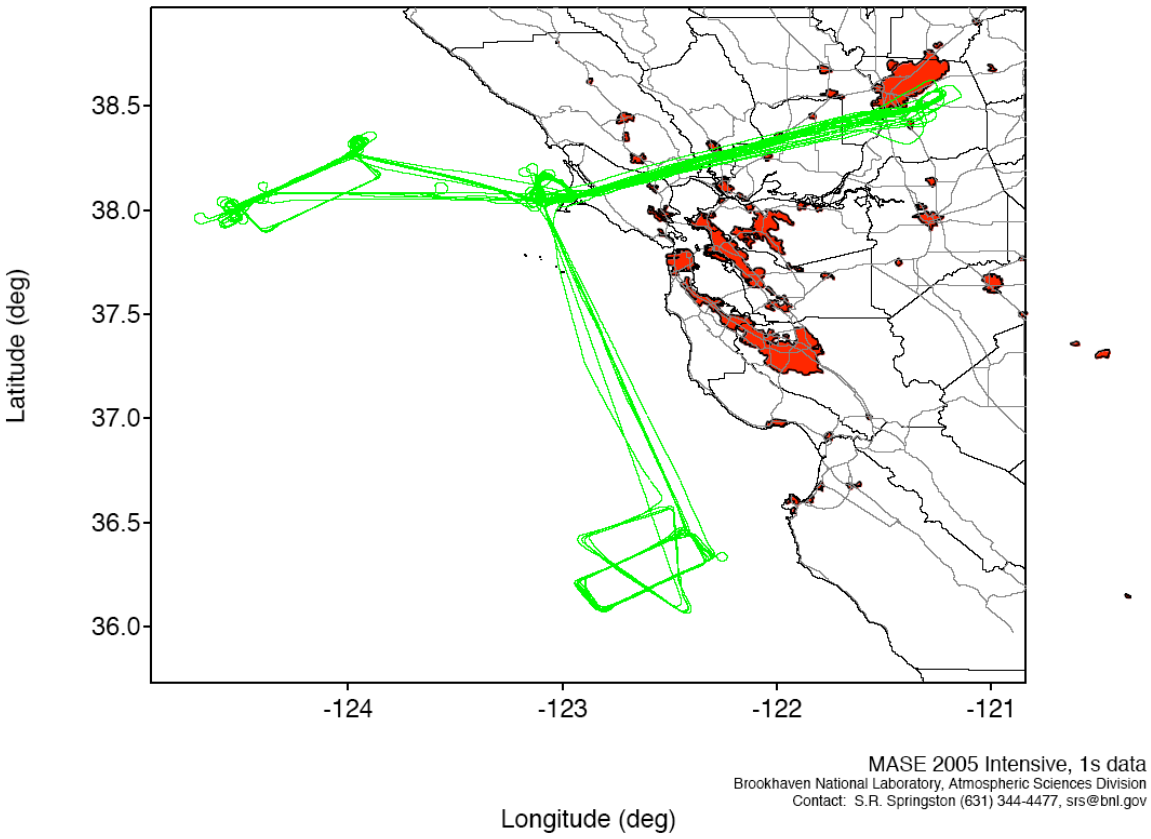

Figure 1. Composite Flight track of all G-1 flights conducted during the 2005 MASE Program. Red coloring indicate areas of high population density.

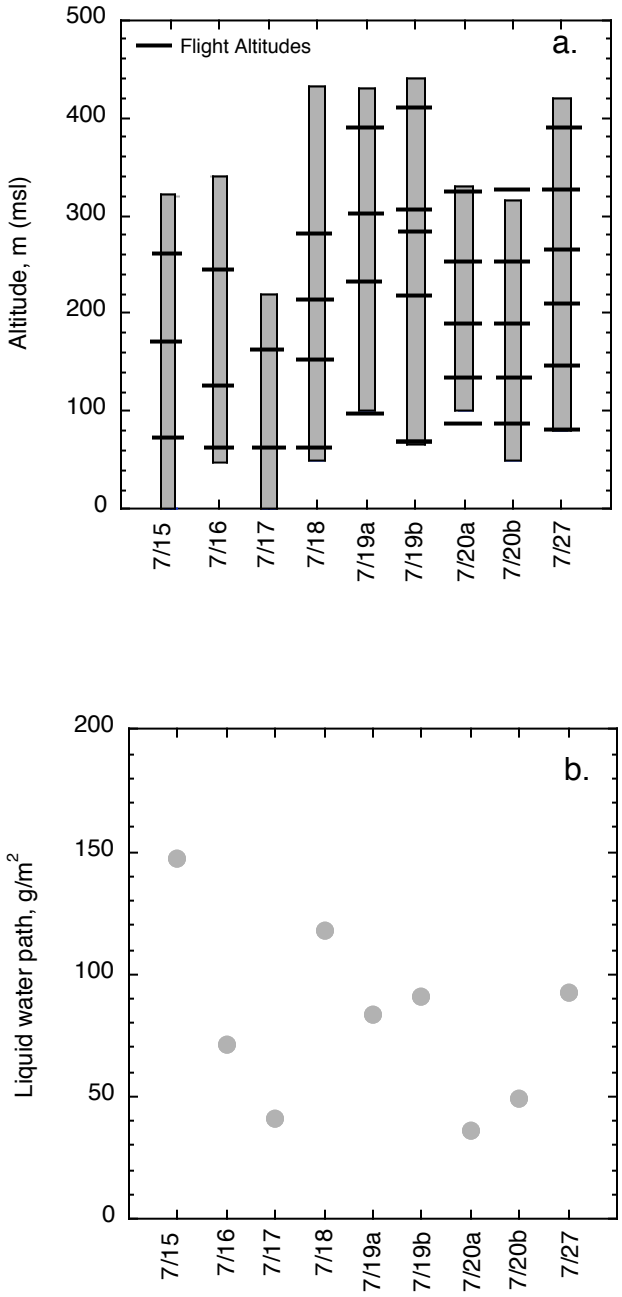

Figure 2a. Cloud vertical extent and G-1 flight sampling altitudes. Vertical extent of clouds indicated by the shaded bar; sampling altitudes by the horizontal lines. b. Cloud liquid water path determined from integration of observed cloud liquid water content.

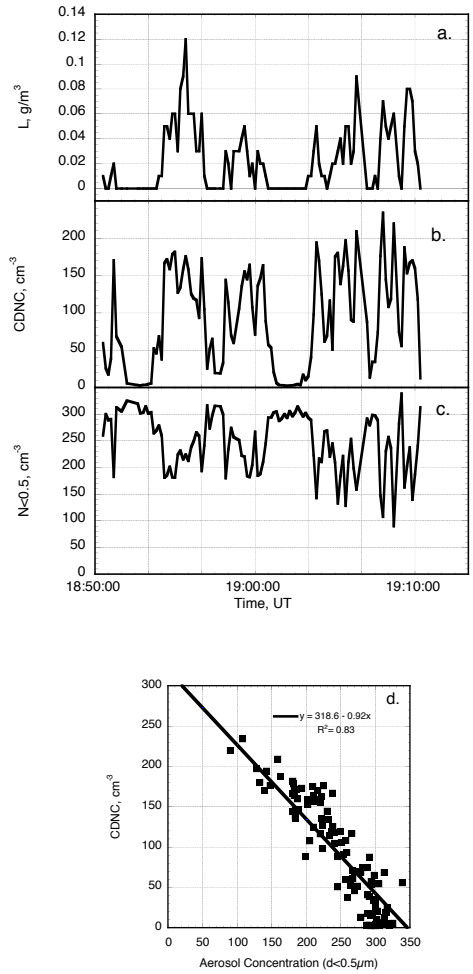

Figure 3. Measurements of cloud properties measured on 7/18 near cloud base in broken clouds. a. Cloud liquid water content. b. Cloud droplet number concentration. c. Concentration of aerosols with d < 0.5 μm. d. Regression plot of CDNC versus concurrently measured aerosol concentration.

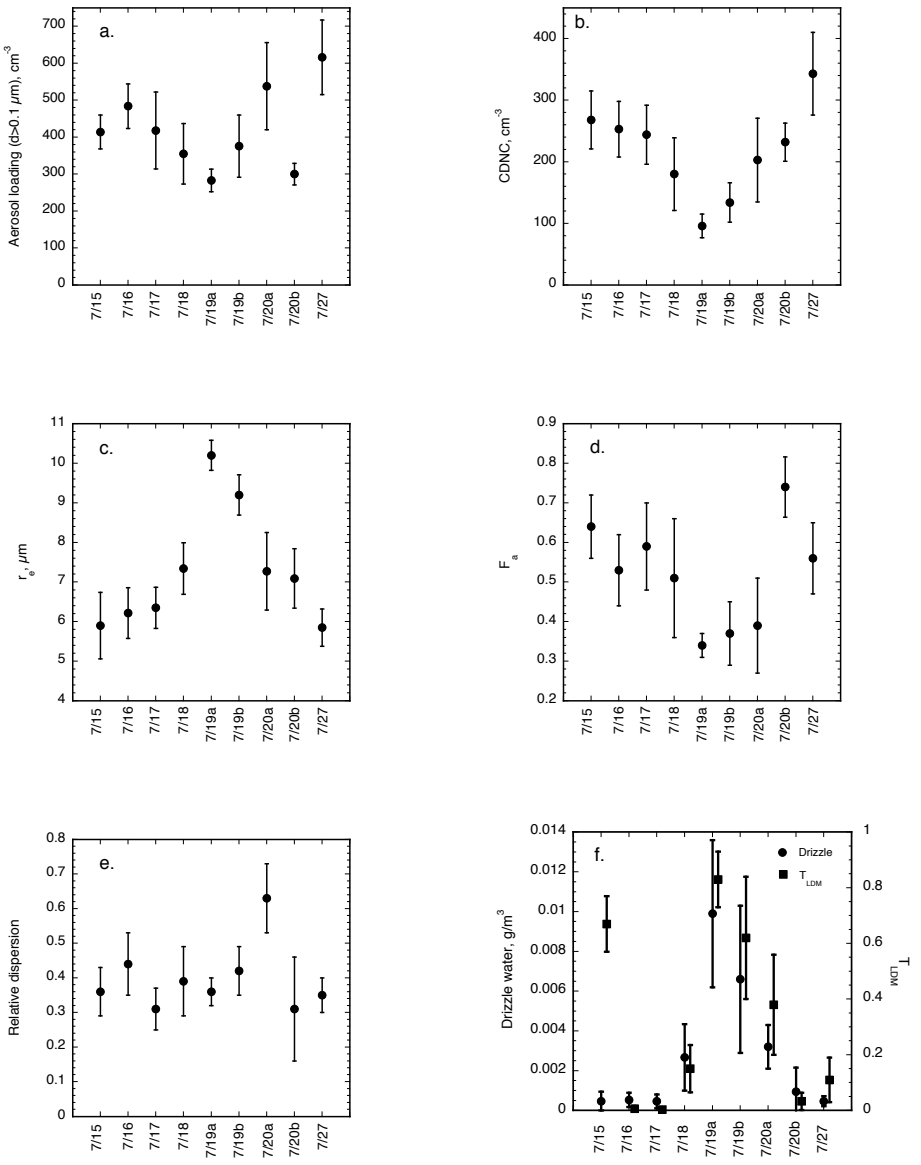

Figure 4. Composite properties of clouds sampled by the G-1 during MASE. Symbols represent quantities averaged over all altitudes flown on the indicated flights. Bars represent standard deviations of the indicated quantities. Points in 4f have been offset for clarity.

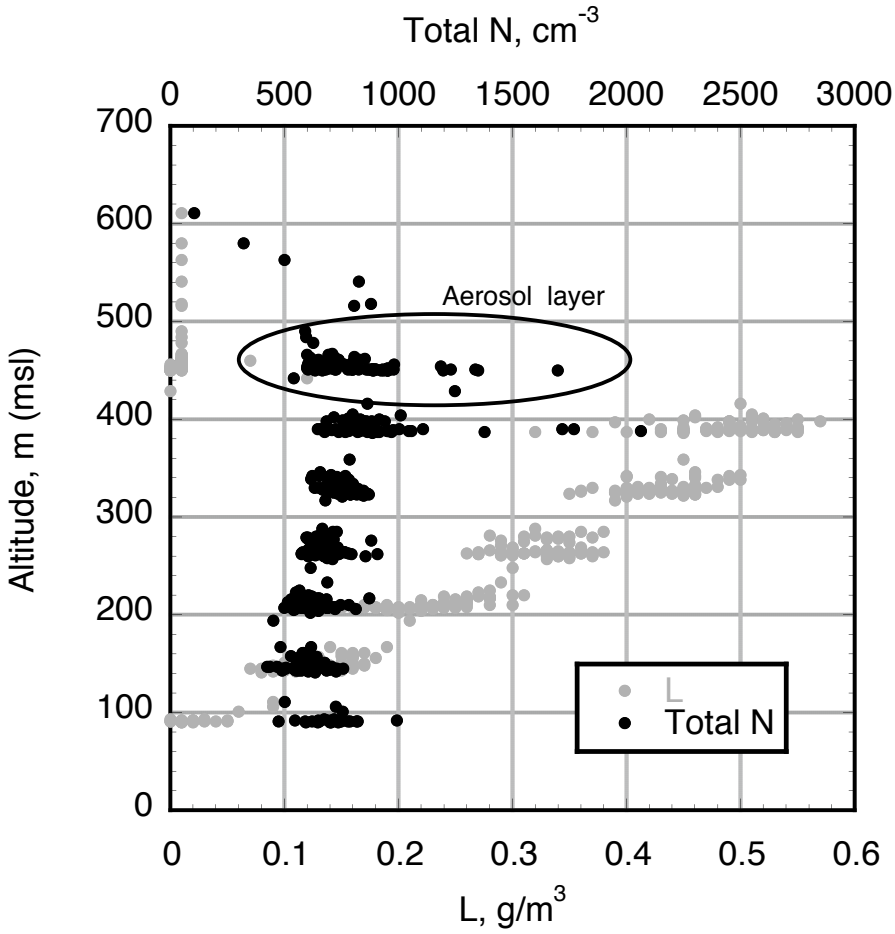

Figure 5. Vertical profile of cloud liquid water content and total particle concentration measured on a flight conducted on 7/27/05 showing the presence of an aerosol layer just above cloud top. Note also the possible entrainment of aerosol into cloud top at an altitude just less than 400 m.

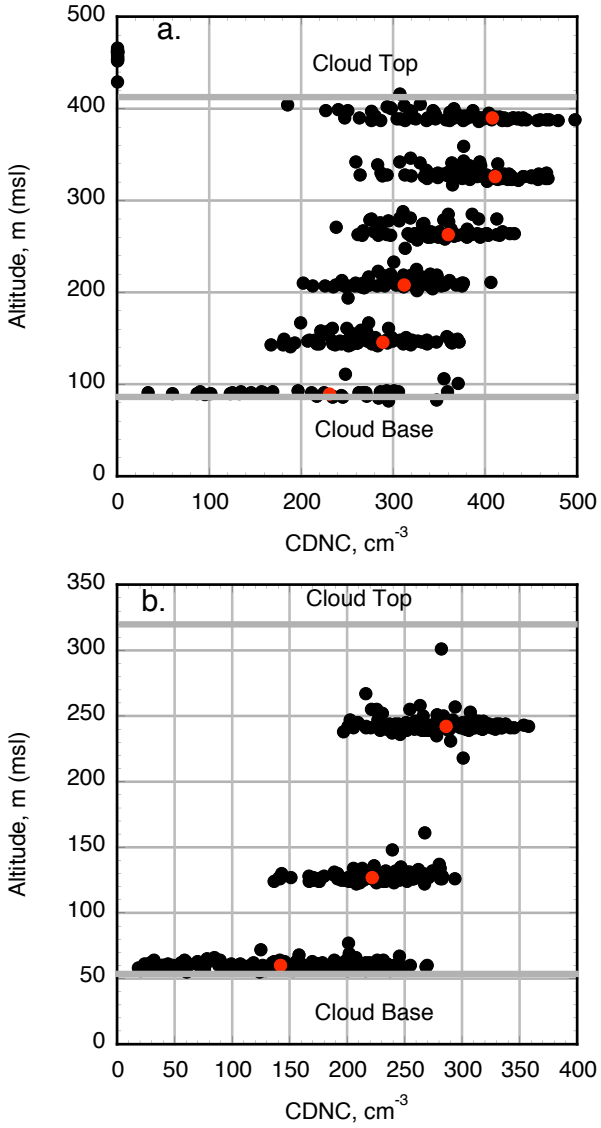

Figure 6. Vertical profiles of cloud droplet number concentration showing an increase in the droplet concentration with height. Black symbols are 10 s averages, red symbols are layer averages. a. Fight of 7/27/05; b. Fight of 7/16/05.

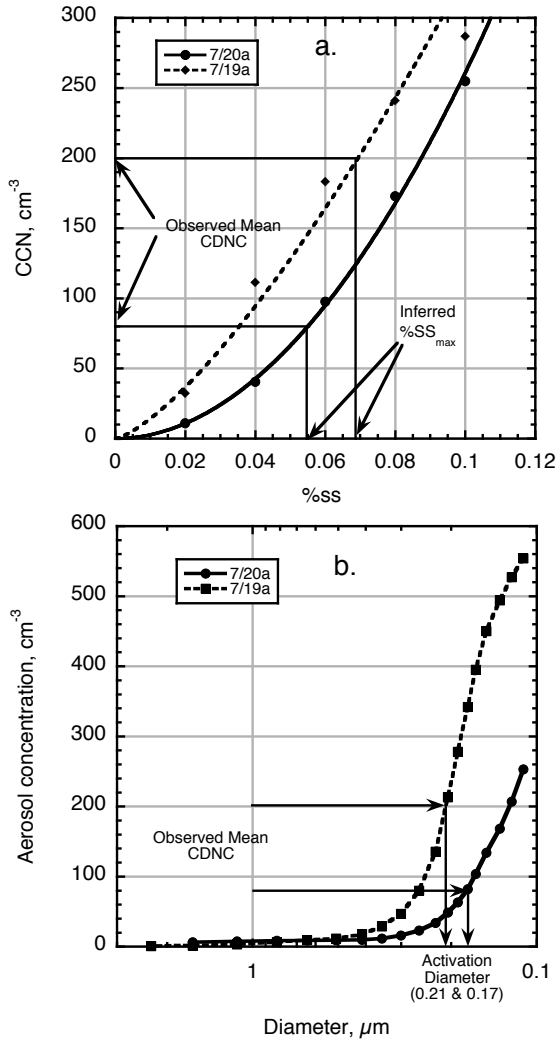

Figure 7. a. Average below cloud supersaturation spectra for the 7/19/05a, and 7/20/05a flights. The observed cloud droplet concentration is the mean value measured just above cloud-base; lines are power-law fits to the data. b. Below cloud cumulative aerosol size distribution for 7/19/05a and 7/20/05a. The average cloud droplet number concentration measured just above cloud base is used to estimate the minimum size particles that had been activated to form cloud droplets.

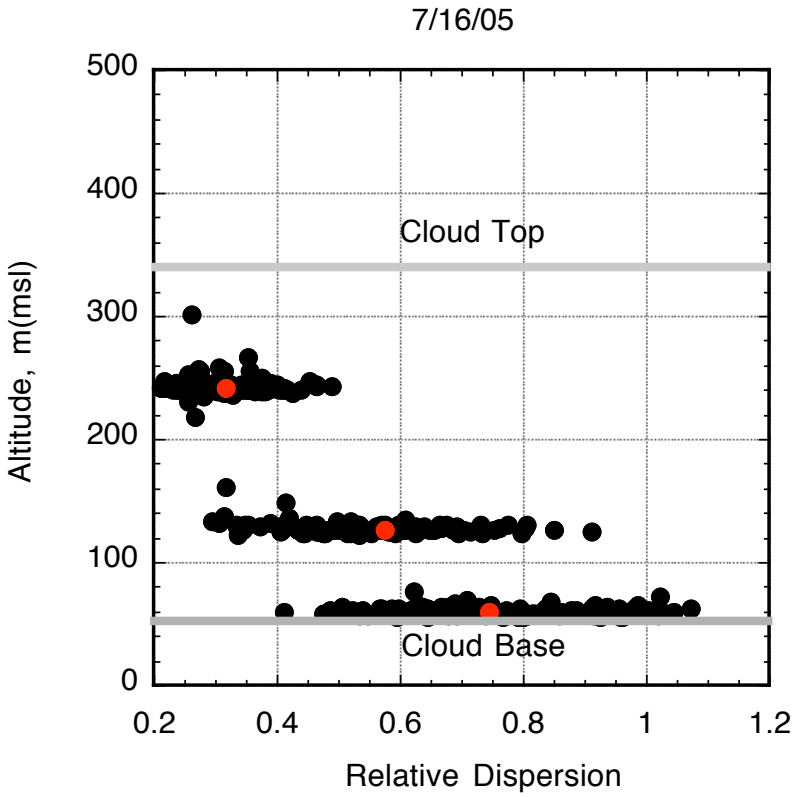

Figure 8. Dispersion of the cloud droplet size distribution for the flight made on 7/16/05. Black symbols are 10 s averages. Red symbols are layer averages.

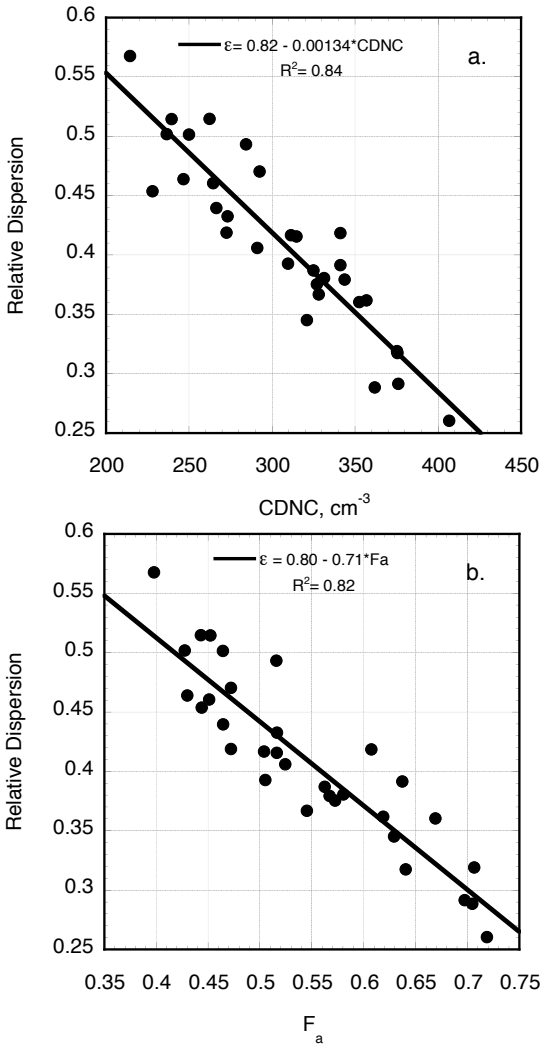

Figure 9. Relative dispersion as a function of a. the measured CDNC for a fixed, and, b. the fraction of particles activated to form cloud droplets for a fixed altitude transect on the flight of 7/27/05.

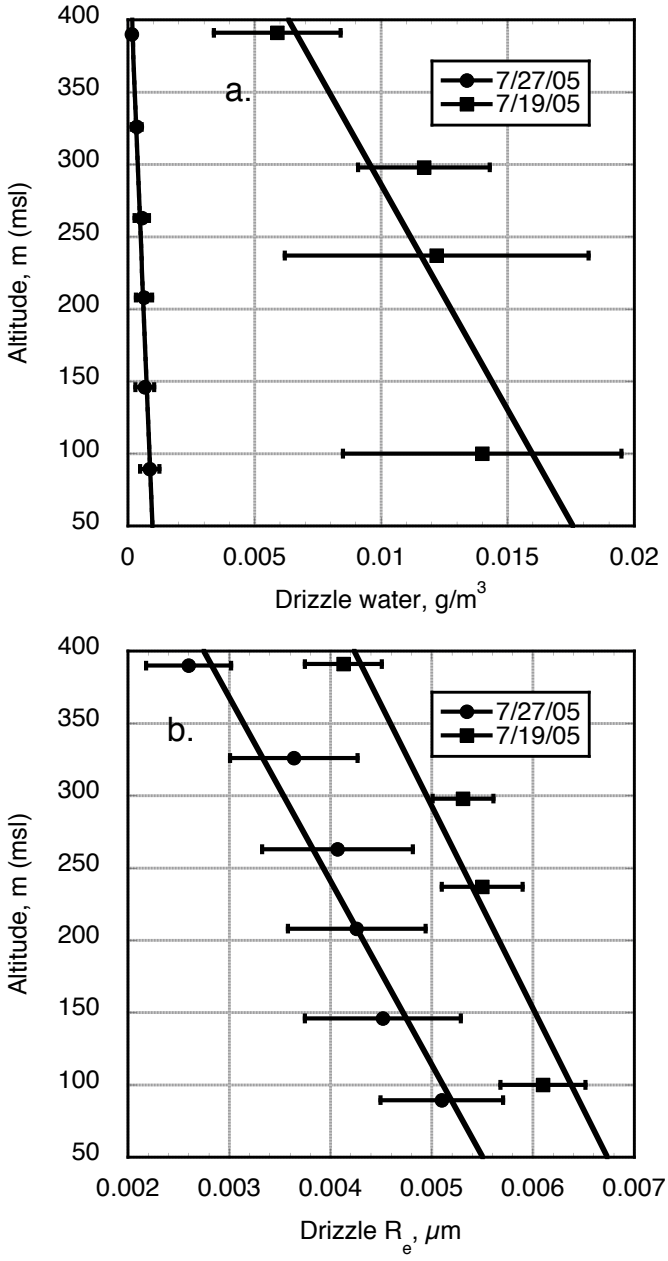

Figure 10. Drizzle properties for flights exhibiting high and low drizzle concentrations. a. Drizzle water content as a function of altitude, and b. Effective drizzle droplet size as a function of altitude for days exhibiting high and low drizzle concentrations.

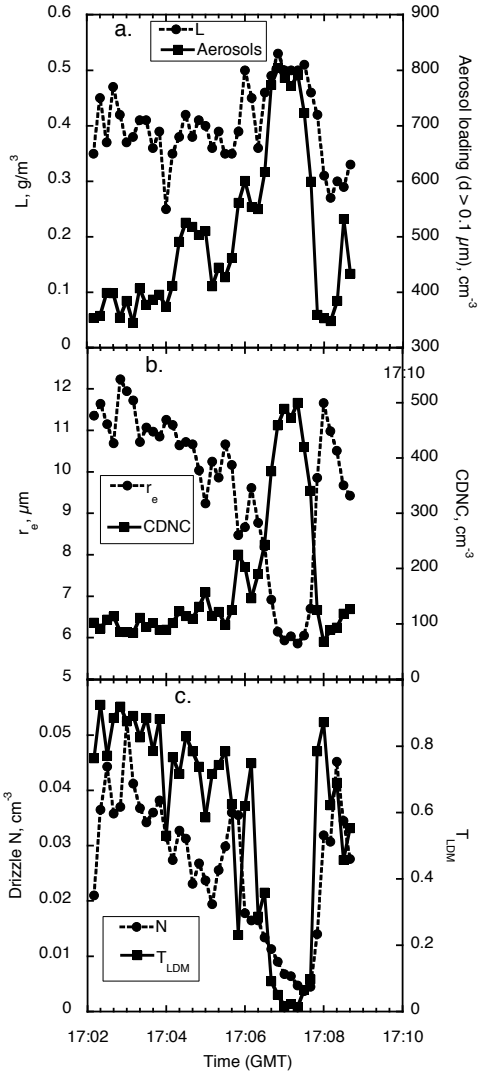

Figure 11. Example of the suppression of drizzle by an aerosol plume encountered on the flight of 7/19/05a over Pt. Reyes. a. Time plot of L and accumulation mode aerosol concentration showing the presence of an aerosol plume at 17:07. b. Time plot of r_e and CDNC showing coincident with the aerosol plume an increase in CDNC and a decrease in r_e. c. Time plot of drizzle water concentration and the threshold function, $T_{LDM,}$ for drizzle formation (see text for details) showing a decrease in the number of drizzle droplets and a decrease in the threshold function coincident with the aerosol plume.

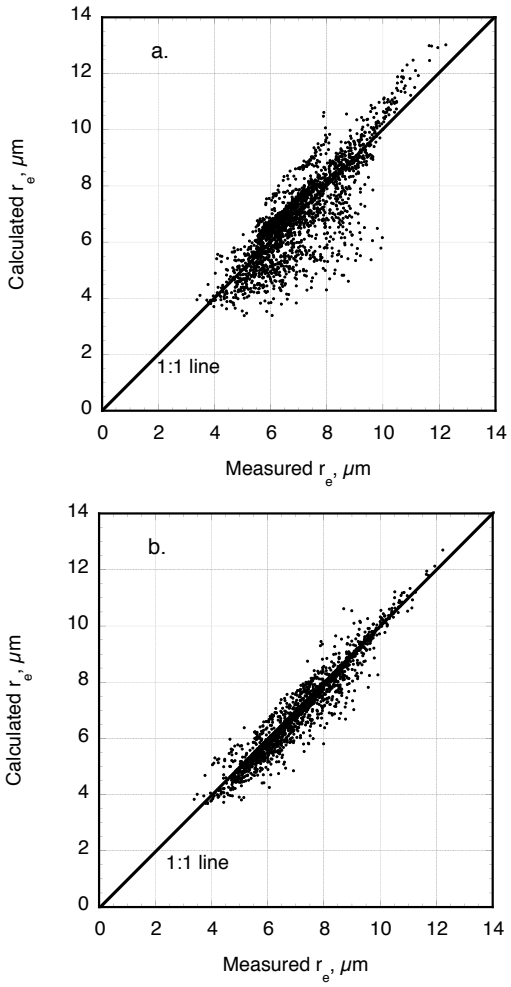

Figure 12. Comparison of r_e computed from measurements of the cloud droplet size distribution to r_e computed from $r_e = 3/(4\pi\rho_w)\beta(L/N)^{1/3}$. a. Assuming β =1.18, and b. Accounting for the dispersion of the droplet size distribution assuming $\beta = (1 + 2\varepsilon^2)^{2/3}/(1 + \varepsilon^2)^{1/3}$. See text for details.

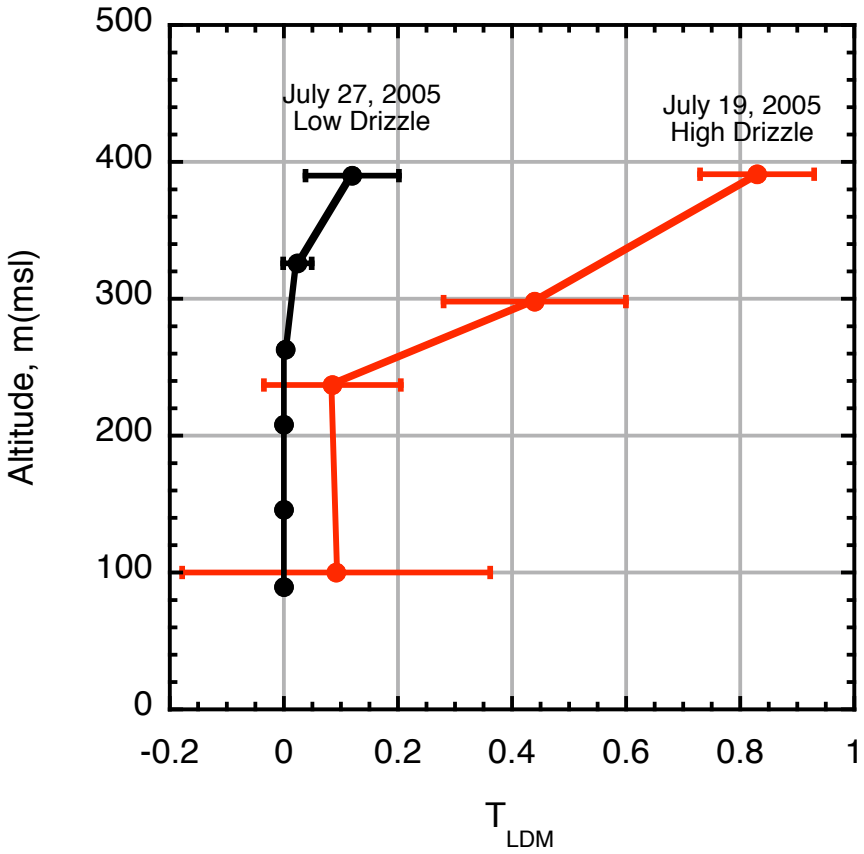

Figure 13. Comparison of the vertical variation in T_{LDM} for a high drizzle day, and a low drizzle day.

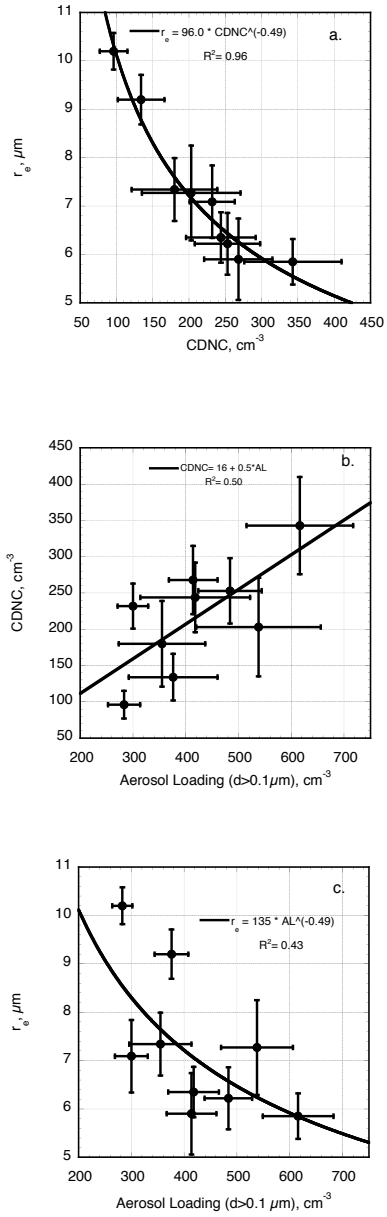

Figure 14. a. Flight averaged r_e as a function of flight averaged CDNC; b. Flight averaged values of the CDNC as a function of aerosol loading; c. r_e as a function of aerosol loading; d. CDNC as function of F_a. Vertical and horizontal bars represent flight-averaged standard deviations.

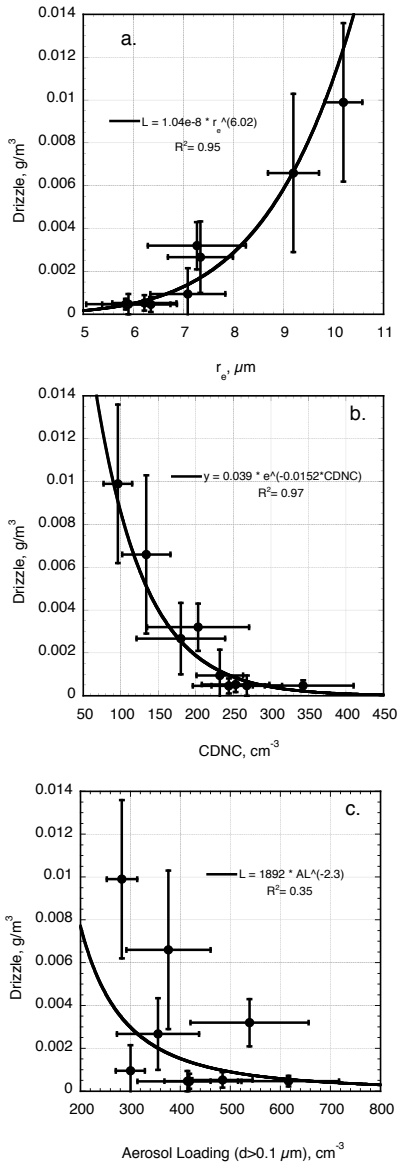

Figure 15. Average drizzle water content as a function of- a. r_e of the cloud droplet size distribution, b. the CDNC; and, c. aerosol loading. Vertical and horizontal bars represent flight-averaged standard deviations.